geosciences

MDPI

Article

In Search for the Limit Between Sedimentology and Stratigraphy: The Case of Zanclean and Gelasian Shallow-Marine Deposits of the Crotone Basin, Southern Italy

Massimo Zecchin [1,*], Mauro Caffau [1] and Octavian Catuneanu [2]

[1] National Institute of Oceanography and Applied Geophysics—OGS, 34010 Sgonico, TS, Italy
[2] Department of Earth and Atmospheric Sciences, University of Alberta, 1-26 Earth Sciences Building, Edmonton, AB T6G 2E3, Canada
* Correspondence: mzecchin@ogs.it

Abstract

The integration of sedimentological and micropaleontological data in the Zanclean and Gelasian shallow-marine deposits of the Crotone Basin (southern Italy) has allowed documentation of meter-to-decameter-scale high-frequency sequences bounded by wave-ravinement surfaces (WRSs), which in turn are composed of meter-scale sedimentological cycles, referred to as bedsets. In contrast to high-frequency sequences, bedsets have a more subtle appearance, and their boundaries exhibit limited lateral extent compared to WRSs. Moreover, the micropaleontological analyses have allowed the definition of three parameters: distal/proximal (D/P: ratio between distal and proximal benthic foraminifera); fragmentation (Fr: percentage of fragmentation of benthic foraminifera); and P/B (ratio between planktonic and benthic foraminifera). In particular, the D/P and Fr allow to recognize uncertainty intervals containing the maximum flooding surface (MFS) of high-frequency sequences, whereas the P/B documents water-depth changes. Unlike in high-frequency sequences, the D/P, Fr and P/B parameters usually do not show appreciable variations associated with bedsets, confirming that the latter are unrelated to shoreline shifts and water-depth variations, but are rather controlled by minor sediment supply and/or wave regime changes. However, in rare cases, the micropaleontological parameters seem to indicate that subtle transgressive-regressive trends and water-depth variations can also be associated with bedset deposition, alluding to a 'grey area' of transition between high-frequency sequences of very small scale and bedsets. Further research is, therefore, needed to constrain the boundary between sedimentology and stratigraphy.

Keywords: stratigraphic sequences; bedsets; micropaleontology; sedimentology; facies analysis

Academic Editor: Michele Morsilli

Received: 19 January 2026
Revised: 18 February 2026
Accepted: 19 February 2026
Published: 21 February 2026

1. Introduction

The separation between stratigraphic and sedimentological cycles is apparently well defined, as the former are usually associated with shoreline transgressions and regressions, whereas the latter, also referred to as bedsets, should only be associated with cyclic processes involving local energy and sediment supply [1–7]. Although systems tracts forming stratigraphic sequences are well recognizable where transgressions and regressions are associated with high-magnitude relative sea-level changes and/or high-magnitude sediment supply variations, meter-to-decameter-scale high-frequency sequences associated

with minor shoreline shifts can be difficult to distinguish from meter-scale bedsets, especially in outcrops with limited areal extent. For this reason, Zecchin et al. [5,6] defined a series of criteria to discriminate between high-frequency sequences and bedsets, which integrate sedimentological, stratigraphic, micropaleontological, mineralogical, and diagenetic approaches. In general, bedset boundaries have a more limited lateral extent and a more subtle physical appearance than the high-frequency sequence boundaries, and the distribution of heavy minerals changes significantly only across stratigraphic boundaries such as wave-ravinement surfaces [5,6].

Despite the progress to date, challenges still remain with respect to the distinction between stratigraphic and sedimentological cycles, as the increasingly finer scales of observation approach the limits of high-resolution stratigraphic studies. This challenge is exacerbated by the common organization of 'bedsets' into 'bedset sets', and the assumption that these units can also be associated with shoreline shifts and minor relative sea-level changes, similar to sequences [8–10]. Based on field data from Pliocene and early Pleistocene shallow-marine deposits of the Crotone Basin (southern Italy; Figures 1 and 2), this study aims to separate stratigraphic from sedimentologic cycles, also employing updated micropaleontological criteria to better define this distinction. These results can help improve the highest resolution sequence stratigraphic analyses of shallow-marine deposits by bringing into focus the objective criteria that define the limit between sedimentology and stratigraphy.

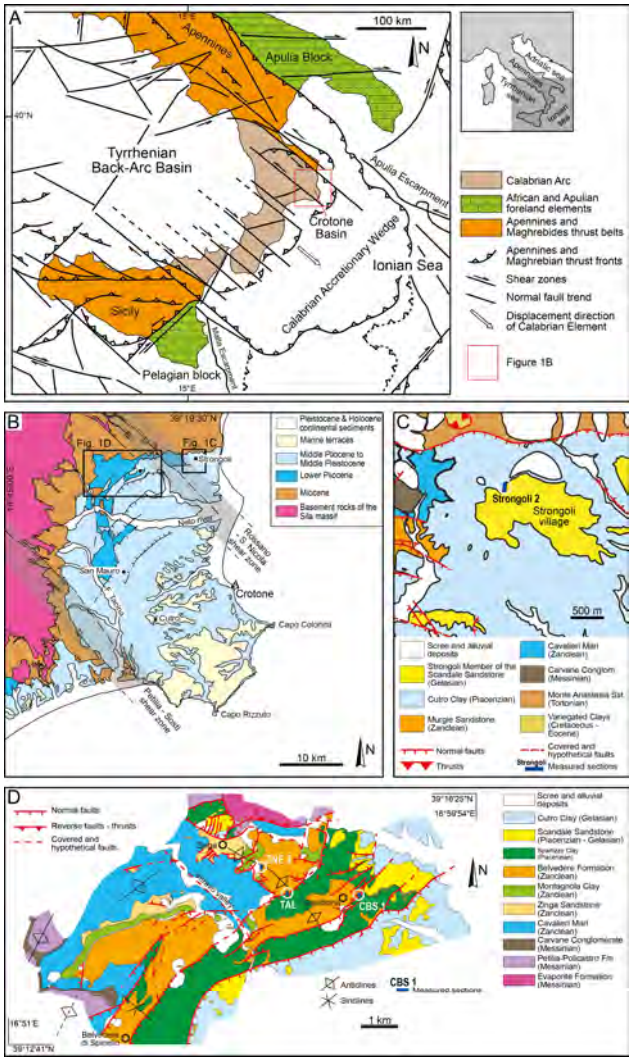

Figure 1. (**A**) Structural map of the Calabrian Arc showing the location of the Crotone Basin (modified from Van Dijk and Okkes [11]). (**B**) Simplified geological map of the Crotone Basin, showing the maps

illustrated in Figure 1C,D (modified from Zecchin et al. [12–14]). (**C**) Geological map of the Strongoli area (Figure 1B for location), showing the position of the Strongoli 2 measured section (modified from Zecchin et al. [13,15]). (**D**) Geological map of the western part of the study area in the Crotone Basin (Figure 1B for location), showing the position of the CBS 1, TAL and ZNE 2 measured sections (modified from Zecchin et al. [14]).

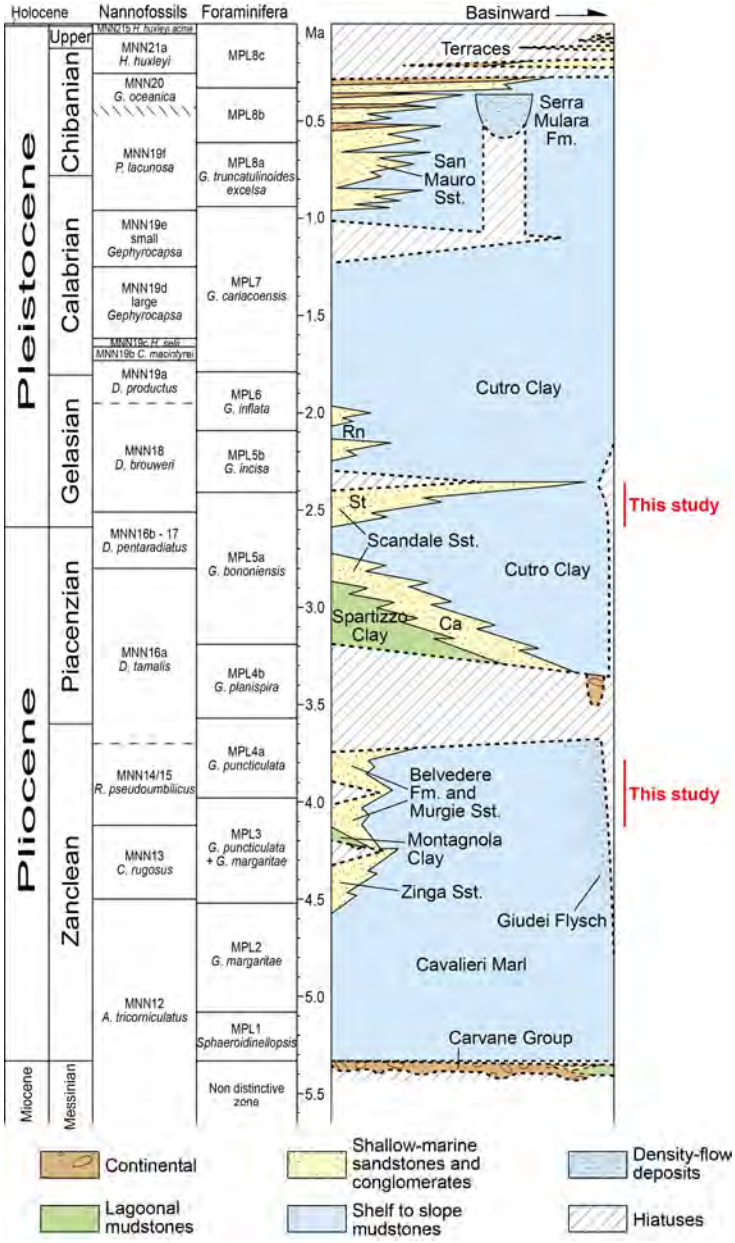

Figure 2. The Plio-Pleistocene part of the sedimentary succession of the Crotone Basin (modified from Zecchin et al. [15]), compared with the IUGS International Chronostratigraphic Chart (https://stratigraphy.org/ICSchart/ChronostratChart2021-05.pdf accessed on 18 February 2026), and the calcareous nannofossil and planktonic foraminifera biostratigraphic schemes [16–19]. The studied succession is part of the Zanclean Belvedere Formation and the Gelasian Strongoli Member of the Scandale Sandstone. Abbreviations: Ca—Casabona Member; Rn—Rocca di Neto Member; St—Strongoli Member.

2. Geological Setting

The Crotone Forearc Basin developed from late Serravallian onwards on the Ionian side of the Calabrian Arc (southern Italy), the latter being located between the southern Apennines and the Sicilian Maghrebides and composed of metamorphic, plutonic and sedimentary units [20–22] (Figure 1A,B). The evolution of the Calabrian Arc was characterized

by an overall SE-ward migration of the whole terrane, concomitant with the subduction of the Ionian oceanic crust and the opening of the Tyrrhenian backarc basin since the Middle Miocene [23–31] (Figure 1).

The sedimentary succession of the Crotone Basin consists of Serravallian to Middle Pleistocene marine, coastal and continental deposits (Figures 1B and 2) and records both tectonic subsidence events and phases of uplift plus basin closure, as well as glacio-eustasy [12,15,32–41]. A generalized tectonic uplift started during the Middle Pleistocene, and this process led to the emergence of the inner part of the basin and the formation of a staircase of marine terraces [42–45].

3. Methods

The considered examples of shallow-marine deposits are described by four detailed measured sections (Figures 1C,D and 3–6). Facies analysis provides the basis for the recognition of facies associations and depositional environments (Table 1), whereas depositional trends and key bounding surfaces are essential to define the sequence stratigraphic framework of the recognized stratigraphic sequences and bedsets.

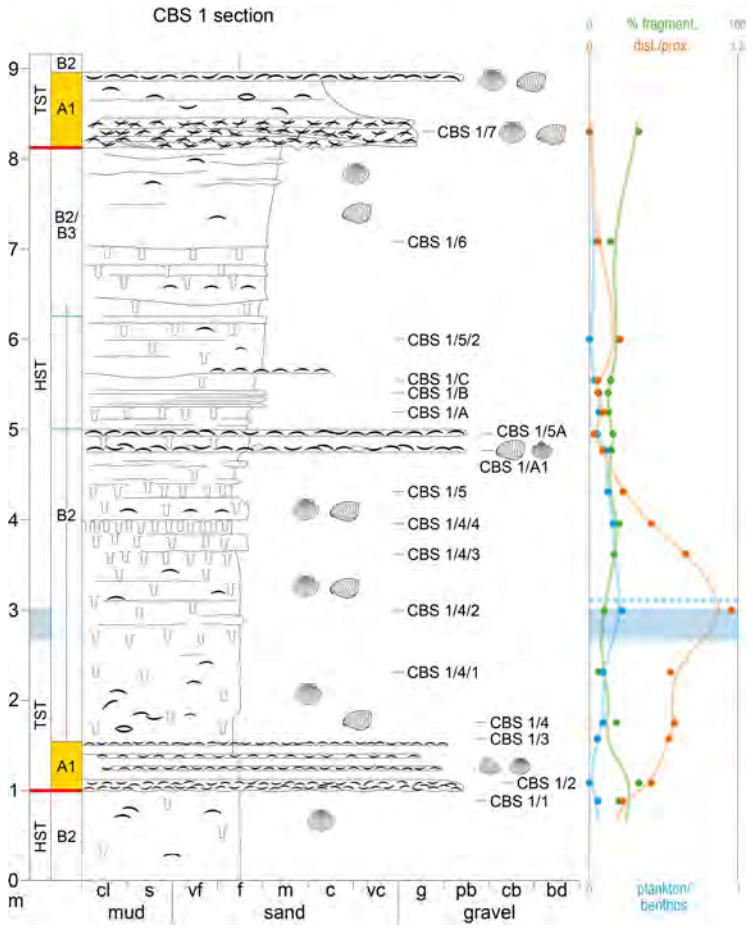

Figure 3. The South Casabona (CBS) 1 section of the Belvedere Formation (Figure 1D for location and Figure 4 for symbols; modified from Zecchin et al. [14]). Sedimentary structures, fossils, samples, facies and facies contacts, sequence stratigraphic surfaces, systems tracts and bedset boundaries are shown. The curves derived from the micropaleontological analysis (% fragmentation, distal/proximal and plankton/benthos, see text) are shown on the right. Two discontinuity surfaces bounding bedsets are found in the middle to upper part of a high-frequency sequence bounded by wave-ravinement surfaces and composed of a transgressive systems tract (TST) and a highstand systems tract (HST). TST and HST are separated by an uncertainty interval inferred to contain the maximum flooding surface, defined on a micropaleontological basis (see text).

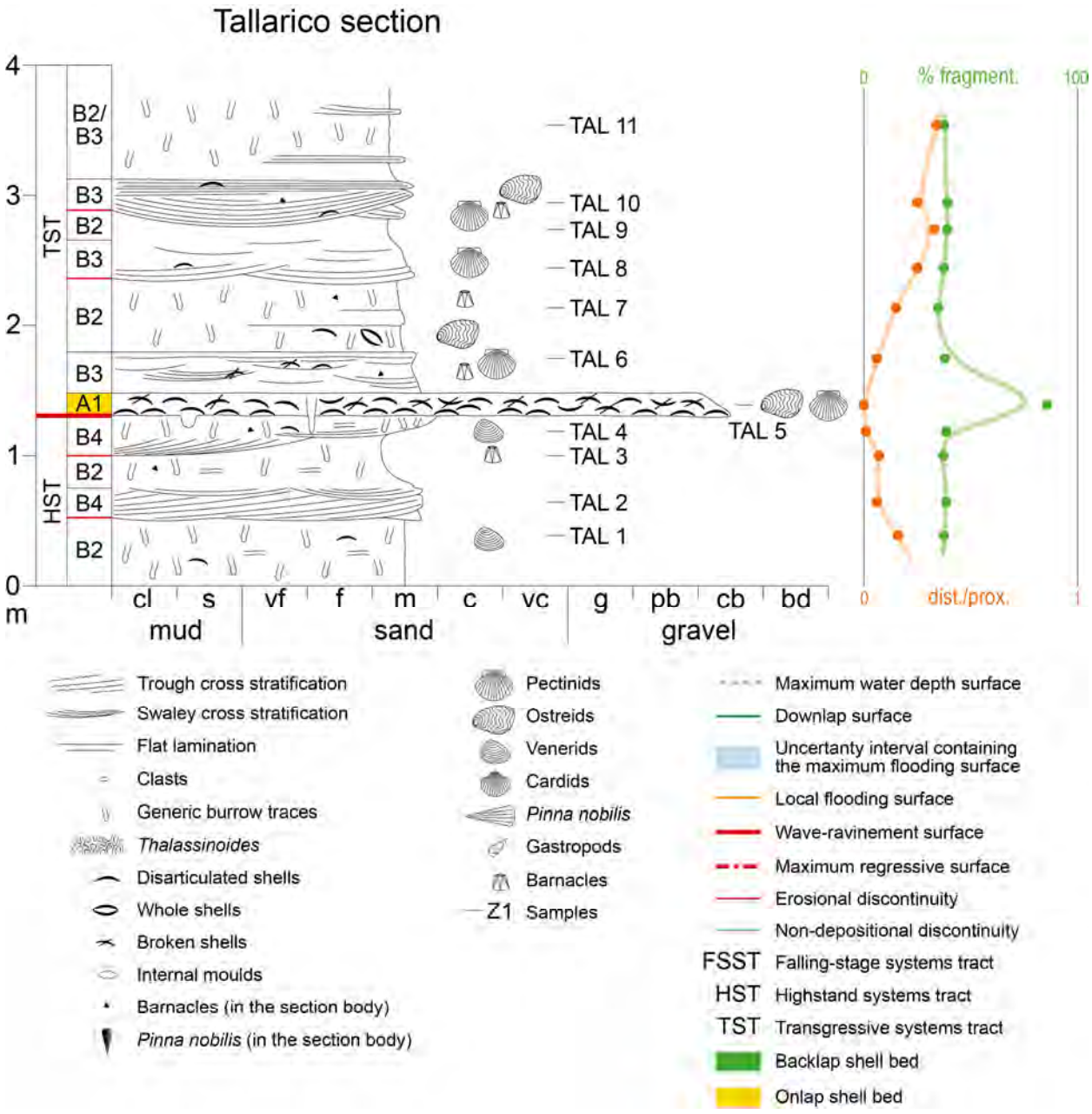

Figure 4. The Tallarico (TAL) section of the Belvedere Formation (Figure 1D for location; modified from Zecchin et al. [5]). Sedimentary structures, fossils, samples, facies and facies contacts, sequence stratigraphic surfaces, systems tracts and bedset boundaries are shown. The curves derived from the micropaleontological analysis (% fragmentation and distal/proximal, see text) are shown on the right. The section documents a wave-ravinement surface separating the HST (below) and the TST (above) of two high-frequency sequences, which are in turn composed of bedsets bounded by erosional discontinuities.

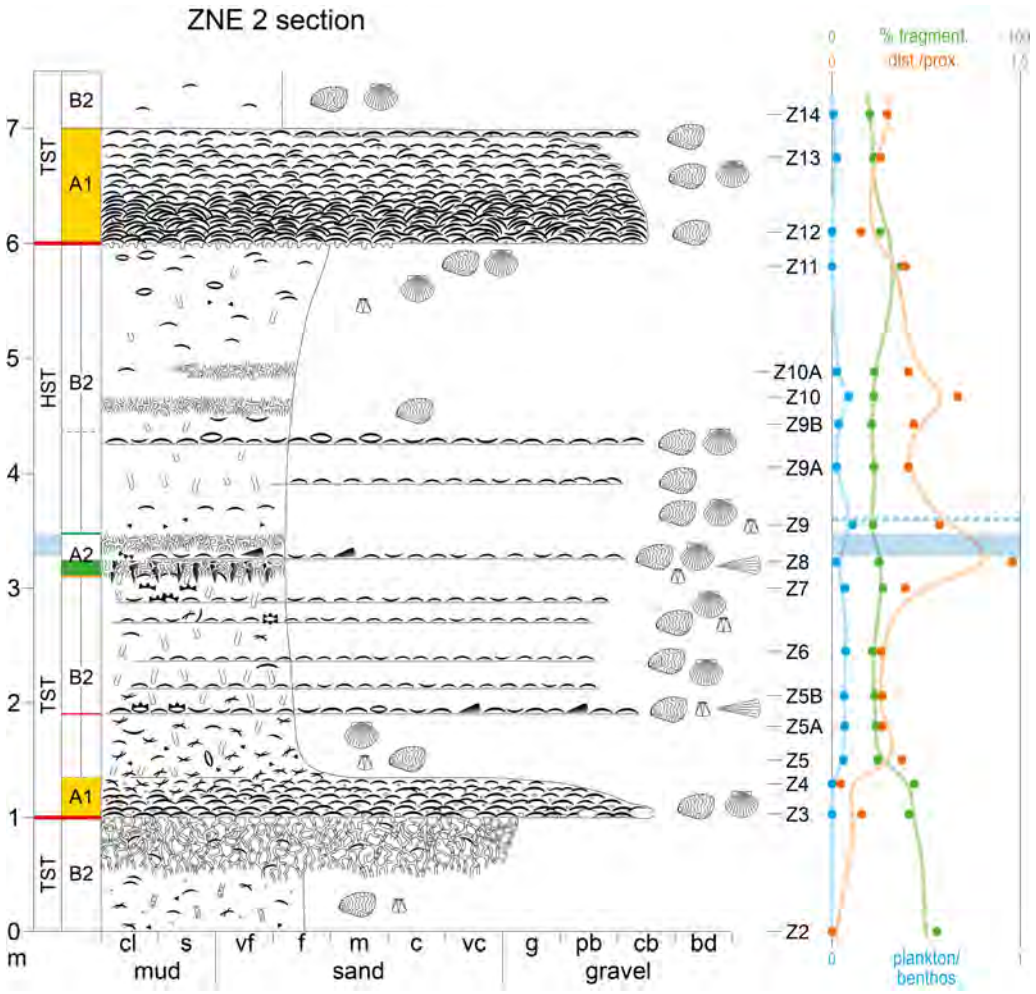

Figure 5. The East Zinga (ZNE) 2 section of the Belvedere Formation (Figure 1D for location and Figure 4 for symbols; modified from Zecchin et al. [14]). Sedimentary structures, fossils, samples, facies and facies contacts, sequence stratigraphic surfaces, systems tracts and bedset boundaries are shown. The curves derived from the micropaleontological analysis (% fragmentation, distal/proximal and plankton/benthos, see text) are shown on the right. A high-frequency sequence bounded above and below by wave ravinement surfaces is documented. The sequence is composed of a TST and an HST separated by an uncertainty interval inferred to contain the maximum flooding surface, defined on a micropaleontological basis (see text). The TST is composed of two bedsets separated by an erosional discontinuity, whereas the HST is composed of two bedsets separated by a non-depositional discontinuity.

Sixty-eight sediment samples were collected along the measured sections (Figures 3–6), and approximately 100 g of sediment was taken from each sample for micropalaeontological analyses. The sample aliquots were dried at 50 °C for 24 h and then treated with hydrogen peroxide (10% vol) for 12 h, in order to remove the organic matter. Samples were then washed through a 125 µm mesh and dried. From the corresponding washing residues, 3 g of sediment was separated, except for the samples of the TAL section, for which, due to the scarcity of specimens, 15 g of sediment was separated. All benthic foraminifera present in this amount of sediment were counted and classified following the taxonomic order of Loeblich and Tappan [46] and subsequent studies (see Section 5).

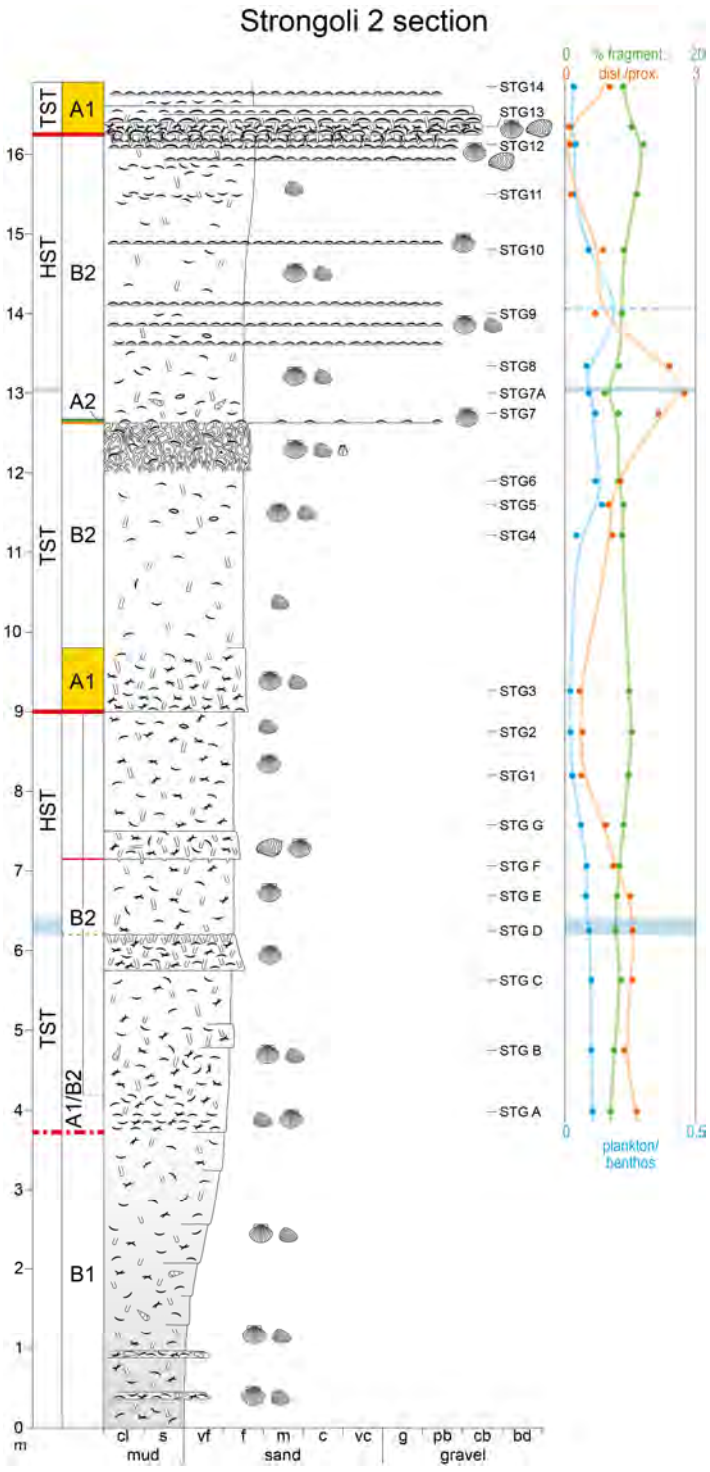

Figure 6. The Strongoli 2 section of the Strongoli Sandstone (Figure 1C for location and Figure 4 for symbols; modified from Zecchin et al. [13]). Sedimentary structures, fossils, samples, facies and facies contacts, sequence stratigraphic surfaces, systems tracts and bedset boundaries are shown. The curves derived from the micropaleontological analysis (% fragmentation, distal/proximal and plankton/benthos, see text) are shown on the right. Two high-frequency sequences bounded by wave-ravinement surfaces, and composed of TST and HST, are documented. TSTs and HSTs are separated by an uncertainty interval inferred to contain the maximum flooding surface, defined on a micropaleontological basis (see text). The HST of the lower sequence is composed of two bedsets separated by an erosional discontinuity.

Table 1. Facies and depositional environments of the studied succession.

Facies Association and Facies	Lithology and Thickness	Sedimentary Structures and Bioturbation	Fossils	Interpretation
A—Condensed shallow-marine				
A1: Wave-dominated shell-rich deposit	Stacked shell beds forming tabular cemented units 0.15 to 1 m thick. The grain size of the matrix ranges from fine-grained siliciclastic sandstone to granule-grade conglomerate and contains shell debris in variable amounts. Cobbles and pebbles of sandstone may be found at the base.	Planar stratification and local swaley cross-stratification. Local upward decreasing shell abundance. Common substrate-controlled *Glossifungites* Ichnofacies at the base. Scattered bioturbation in the body. Erosional base and sharp to gradual upward transition into Facies B2.	Ostreids, pectinids and minor venerids (usually disarticulated and broken), usually convex-up arranged but also concave-up arranged. Shells form stacked horizontal sheets or can be chaotically packed.	Shoreface deposit recording low net sedimentation rates, high-energy wave action and high production of mollusk communities [5,13,14,47–50].
A2: Surface-related shell bed	Shell-rich fine-grained siliciclastic sandstone, 1 shell to 0.4 m thick.	Diffuse bioturbation and shell layers in the thicker beds, common substrate-controlled *Glossifungites* Ichnofacies up to 0.5 m deep at the base. Sharp base and top.	Disarticulated and locally broken pectinids, ostreids and minor venerids and barnacles, aligned on the basal surface or in layers within the thicker beds. Local presence of *Pinna nobilis* in life position at the base.	Community shell concentration recording low energy levels and sediment starvation in the distal lower shoreface [14,47,49,51,52].
B—Siliciclastic shoreface				
B1: Sand and mud	Very fine-grained quartz sandstone with silt matrix 3–4 m thick	Structureless, rare cm-scale sand layers, sparse bioturbation. Gradational upper boundary with Facies B2.	Venerids, pectinids and gastropods	Shoreface–shelf transition [13,47,53,54].
B2: Burrowed sandstone	Fine- to medium-grained siliciclastic sandstone up to 4.5 m thick.	Mostly structureless to planar stratified, scattered bioturbation, locally intense. The boundaries are sharp to gradual with Facies A1, A2, B1 and B3.	Sparse disarticulated (whole in places) pectinid, ostreid and venerid shells. Barnacles are also common. Gastropods, and disarticulated cardids and *Pinna nobilis* are locally present.	Lower shoreface and low-energy middle/upper shoreface [5,13,14,47,54,55].

Table 1. *Cont.*

Facies Association and Facies	Lithology and Thickness	Sedimentary Structures and Bioturbation	Fossils	Interpretation
B3: Swaley cross-stratified to planar-laminated sandstone	Medium- to very coarse-grained siliciclastic sandstone up to 0.4 m thick.	Swaley cross-stratification to planar lamination. Scattered bioturbation. Sharp lower boundary and sharp to gradual upper boundary with Facies B2. Facies B2/B3 transitions with intermediate characteristics are also present.	Disarticulated and locally broken pectinid and ostreid shells, mainly convex-up arranged. Occasional barnacles.	Storm-dominated middle shoreface [5,14,56–58].
B4: Mixed trough and swaley cross-stratified sandstone	Medium-grained siliciclastic sandstone up to 0.3 m thick.	Trough and swaley cross-stratification. Erosional lower boundary and gradual upper boundary with Facies B2.	Barren.	Storm-dominated middle-upper shoreface transition [5,53,59,60].

4. The Studied Succession

4.1. Sedimentary Units

The deposits considered for this study are part of the Zanclean Belvedere Formation and the Gelasian Strongoli Member of the Scandale Sandstone (simply referred to herein as the Strongoli Sandstone [13,32]; Figures 1C,D, 2 and 7), which were largely documented by Zecchin et al. [5,13,14,47] and references therein, to whom the reader is referred for a complete description.

In brief, the shallow-marine Belvedere Formation (Figures 2 and 7A) is tens to hundreds of meters thick and is composed of siliciclastic and bioclastic deposits accumulated within half-graben sub-basins [5,12,14,15,34,35,47,61]. Fault-controlled subsidence led to a marked aggradational component that affords the recognition of meter- to decameter-scale sequences, which are inferred to have been controlled by Milankovitch-driven climatic and sediment supply changes [5,14,47]. Typically, these sequences are bounded by wave-ravinement surfaces (WRS) and consist of a transgressive systems tract (TST), containing shell-rich deposits, and a mainly siliciclastic highstand systems tract (HST) (Figures 3–5).

The Strongoli Sandstone (Figures 2 and 7B) is up to 70 m thick and pinches out basinward within shelf deposits (the Cutro Clay, Figures 2 and 7B) [13,15,35,47,62]. An overall regressive trend, from shoreface–shelf transition to upper shoreface settings, is shown by the unit [13]. The middle to upper part of the Strongoli Sandstone is composed of six high-frequency sequences up to 7 m thick, which exhibit an architecture similar to that of the Belvedere Formation (Figure 6) and are inferred to be controlled by Milankovitch cyclicity [47].

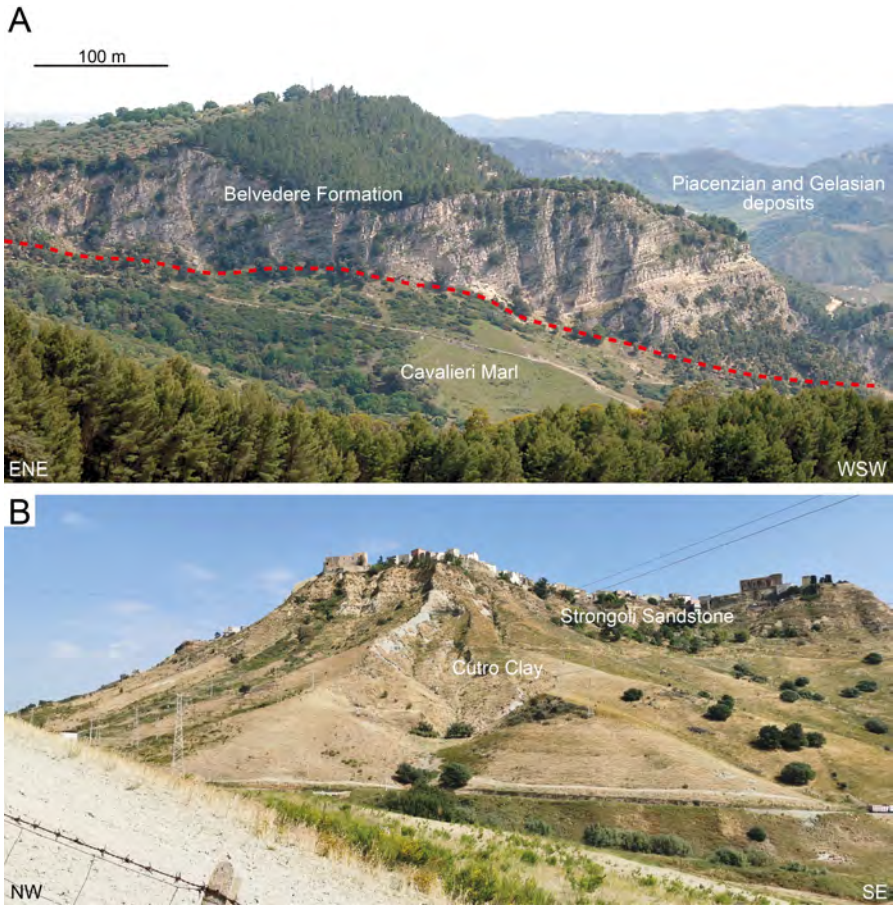

Figure 7. (**A**) Example of a large outcrop of the Zanclean, shallow-marine Belvedere Formation, separated from the Zanclean Cavalieri Marl by a normal fault (red dotted line; Figures 1D and 2). (**B**) Piacenzian to Gelasian normal regressive succession showing the transition between the shelf Cutro Clay and the shallow-marine Strongoli Sandstone (Figures 1C and 2).

4.2. Facies and Depositional Environments

Facies and interpreted depositional environments for the studied deposits of both the Belvedere Formation and the Strongoli Sandstone are illustrated in Table 1. Further facies details of these units are reported by Zecchin et al. [5,13,14,47]. Two facies associations were recognized: condensed shallow-marine (A) and siliciclastic shoreface (B) (Table 1). Facies association A includes shell-rich deposits recording net sediment bypass and/or starvation, whereas facies association B contains mostly siliciclastic shoreface deposits.

The shell-rich Facies A1 (Figures 3–6 and 8A) reflects depositional conditions characterized by high energy levels due to the action of waves and storm flows, leading to sediment bypass during coastal retreat, as well as trophic conditions favoring the development of rich mollusk communities [5,14,47]. Shells are commonly arranged in layers. Facies A1 is erosionally based, and commonly typified by the substrate-controlled *Glossifungites* Ichnofacies (Figures 4, 5 and 8A). A pebble-to-cobble-sized lag can be rarely found at the base (Figure 5). In some cases, deposits with intermediate features between Facies A1 and the siliciclastic Facies B2 (see below) have been observed (Figure 6). Facies A2 is typically thin (no more than 0.4 m), burrowed, exhibits the *Glossifungites* Ichnofacies at its sharp base, and is locally associated with *Pinna nobilis* shells in life position, all features that reflect low energy levels and overall sediment starvation (Figures 5, 6 and 8B [14,47]).

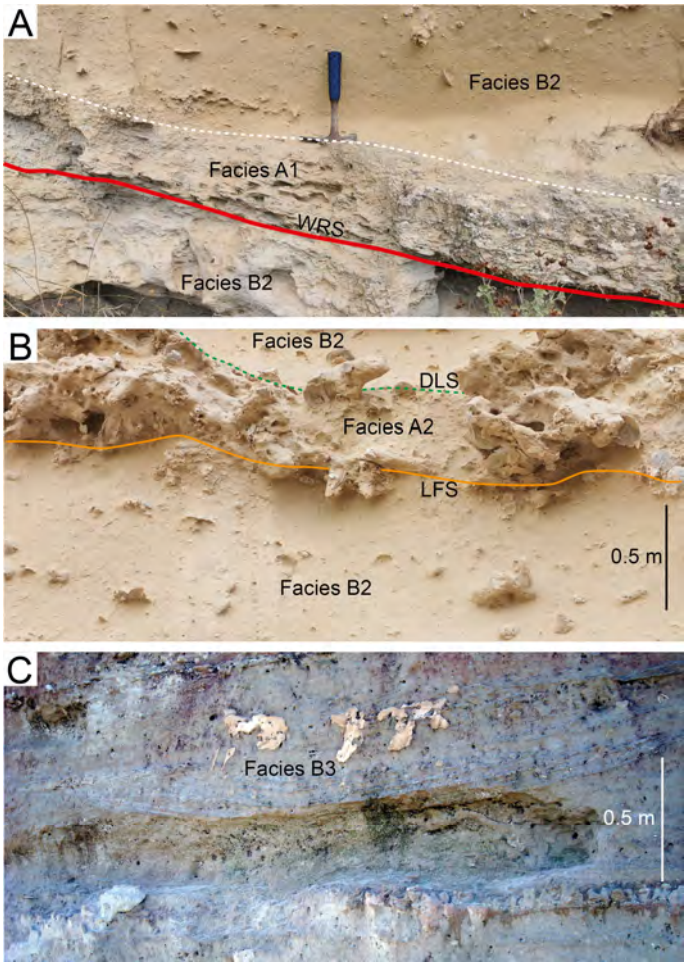

Figure 8. (**A**) The shell-rich Facies A1 in the ZNE 2 section (Figure 5), between intervals of the siliciclastic Facies B2. Facies A1 is bounded below by a wave-ravinement surface (WRS) that truncates the underlying deposits. The underlying Facies B2 is penetrated by burrows belonging to the *Glossifungites* Ichnofacies. (**B**) Burrowed interval belonging to Facies A2 in the ZNE 2 section (Figure 5), bounded below by a local flooding surface (LFS) and above by a downlap surface (DLS) (see text). Facies A2 is encased in Facies B2. Note two *Pinna nobilis* shells in life position that descend from the LFS. (**C**) Swaley cross-stratification of Facies B3 in the TAL section (Figure 4).

Facies association B documents a regressive shoreface succession (e.g., [53]). Facies B1 (Figure 6) is characterized by lower grain size and energy conditions, reflecting shoreface–shelf transition depositional settings. Facies B2, characterized by diffuse bioturbation and local shell layers (Figures 3, 4, 5, 6 and 8A,B), is the most common facies in the studied deposits and documents accumulation in lower shoreface settings or in middle to upper shoreface settings typified by temporarily decreased energy conditions [5,13,14,47]. Higher energy levels are documented by swaley cross-stratified (Facies B3; Figures 4 and 8C) and mixed trough and swaley cross-stratified (Facies B4; Figure 4) sandstones, accumulated, respectively, in wave-dominated middle shoreface and transitional middle-upper shoreface settings [5,14,47].

5. Micropaleontological Analysis

The dominance of shallow-water species of benthic foraminifera in the sediment samples (Supplementary data) is justified by the proximal depositional settings of the studied deposits. These species are represented by *Ammonia parkinsoniana*, *A. tepida* and *Elphidium* spp. [63–66] (see Supplementary data). The abundance of more distal species, such as *Amphycorina scalaris*, *Bolivina* spp., *Bulimina* spp., *Cibicidoides pseudoungerianus*,

Globobulimina affinis, *Lenticulina* spp., *Nonion boueanum*, *Nonion faba*, *Planulina ariminensis*, *Uvigerina* spp., increases in deeper settings (e.g., [67–69]) (Supplementary data). For the TAL section (Figure 4), showing abundant proximal facies (Facies B3 and B4), *Ammonia beccarii*, *Biasterigerina planorbis*, *Cibicides refulgens*, *Lobatula lobatula* and *Nonionella turgida* are considered as relatively distal species (Supplementary data) [68,70–72]. In contrast, if present, these species are not considered as 'distal' in the other sections, where lower shoreface deposits containing more distal species are found. Planktonic foraminifera are scarce or absent in all sections. Reworked specimens of both benthic and planktonic foraminifera are abundant and must be excluded from the calculation of the parameters.

Following Zecchin et al. [13,14,47], three parameters were calculated on the basis of the micropaleontological analysis: the '% fragmentation' (Fr; the percentage of fragmentation benthic foraminifera for each sample), the 'distal/proximal' (D/P; the ratio between relatively distal and proximal species of benthic foraminifera for each sample), and the 'plankton/benthos' (P/B; the ratio between the number of planktonic foraminifera and benthic foraminifera for each sample) (Figures 3–6). The Fr considers specimens fragmented naturally, thus excluding those resulting from the preparation process [14]. In particular, two or more fresh fragments of the same specimen in the slide are assumed to be the result of the preparation and are therefore included in the count of whole specimens. This is because it is unlikely that fragments of the same specimen, produced by local high-energy environmental conditions, are sedimented together [14]. The evaluation of this parameter requires criteria consistency; if specimens with less than a given percentage of preservation are considered as fragmented, this must be valid for all samples [73]. It is known that the Fr parameter reflects the environmental energy, in turn linked to changes in wave/current power and/or shoreline shifts, whereas the D/P parameter is thought to be sensitive to sedimentation rates linked to shoreline shifts [13,14,47,73]. Maximum values of the D/P parameter are close to minimum values of the Fr parameters (Figures 3, 5 and 6), reflecting maximum flooding conditions. In contrast, higher values of the P/B parameter indicate maximum water-depth conditions, which usually follow (occur later than) maximum flooding conditions (the maximum water-depth surface, MWDS [13,14,47,73]) (Figures 3, 5 and 6).

Due to the way the D/P parameter is defined, the species of relatively distal and proximal benthic foraminifera may vary case by case, in relation to the taxa present in a given succession, as well as the position of a given section along depositional dip [73]. Considering the available literature [63–72], for the CBS 1, ZNE 2 and Strongoli sections (Figures 3, 5 and 6), the D/P parameter is calculated as follows:

D/P = (% *Amphycorina scalaris*, % *Bolivina* spp., % *Bulimina* spp., % *Cibicidoides pseudoungerianus*, % *Globobulimina affinis*, % *Lenticulina* spp., % *Nonion boueanum*, % *Nonion faba*, % *Planulina ariminensis*, % *Uvigerina* spp.)/(% *Ammonia tepida* + % *Ammonia parkinsoniana* + % *Elphidium* spp.).

For the TAL section (Figure 4), the D/P parameter is calculated as follows:

D/P = (% *Ammonia beccarii* + % *Biasterigerina planorbis* + % *Cibicides refulgens* + % *Lobatula lobatula* + % *Nonionella turgida*)/(% *Ammonia parkinsoniana* + % *Elphidium* spp.).

The Fr, D/P and P/B parameters are shown along the measured sections as average curves interpolating the measured points (Figures 3–6). An uncertainty interval between Fr minima and D/P maxima, within which the maximum flooding surface (MFS) should lie, can be defined within each sequence [13,14,47,73] (Figures 3, 5 and 6). The uncertainty interval is the best way to pick the cryptic MFS, which usually lacks any physical diagnostic features.

6. Cyclicity of the Sedimentary Succession

6.1. High-Frequency Sequences

The high-frequency sequences of the studied deposits were largely described by Zecchin et al. [13,14,47]. These sequences (5 to 7 m thick in the present examples; Figures 3–6 and 9) are bounded by wave-ravinement surfaces (WRS) and are typically composed of a shell-rich (mainly Facies A1 and B2 with occasional Facies B3) transgressive systems tract (TST) and a mostly siliciclastic (mainly Facies B2 and B3 with minor Facies B4) highstand systems tract (HST). The WRS can be marked by the *Glossifungites* Ichnofacies and by shell beds (Facies A1) produced by sediment bypass during shoreface retreat (the onlap shell bed; OSB [48]), and by lag deposits (Figures Figure 3–6 and 8A). WRSs are close to Fr maxima and D/P minima (Section 5) (Figures 3, 4 and 6), except in cases where the WRS overlies proximal deposits of the underlying sequence, characterized by higher values of Fr and lower values of D/P (Figure 5). MFSs are cryptic and are placed roughly in the middle of sequences; they lie within the uncertainty interval between D/P maxima and Fr minima (see Section 5 and Zecchin et al. [13,14,47,73]) (Figures 3, 5 and 6). Uncertainty intervals containing the MFS range between a few cm and 0.3 m in thickness and cannot be recognized by sedimentological criteria. However, the local flooding surface (LFS), produced between lower shoreface and inner shelf settings by sediment starvation during late transgression, is a facies contact usually found just below the uncertainty interval (Figures 5, 6 and 8B). LFSs can be marked by the *Glossifungites* Ichnofacies and relatively thin shell beds (the backlap shell beds; BSB) that may contain shells in life position in relatively distal settings (Facies A2) [48,74,75] (Figures 5, 6 and 8B). The downlap surface (DLS; Figures 5 and 8B) is recognizable at the top of the BSB or, more generally, of the condensed section (CS), and marks the base of the HST prograding shallow-marine wedge [48]. The maximum water-depth surface (MWDS) is a cryptic surface picked at the P/B maxima (Figures 3, 5 and 6), which is inferred to coincide with the deepest bathymetry within a sequence [14,73]. The MWDS is usually placed just above the MFS, in the early HST (Figures 3, 5 and 6).

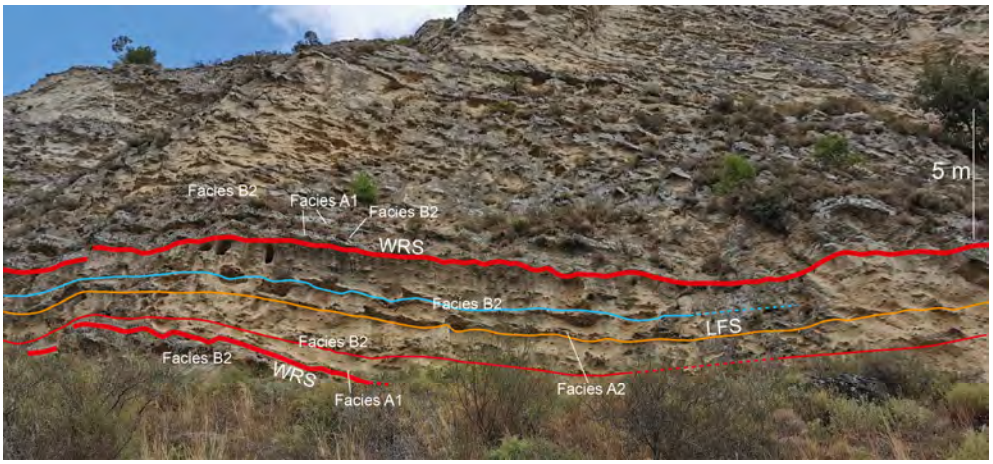

Figure 9. View of the high-frequency sequence documented by the ZNE 2 section (Figures 1D and 5), bounded at the base and at the top by wave-ravinement surfaces (WRS) (see Table 1 for facies code). A local-flooding surface (LFS), close to maximum flooding conditions (see text), is found in the middle of the sequence. A bedset boundary represented by an erosional discontinuity (thin red line) is found in the lower, transgressive part of the sequence, whereas another bedset boundary, represented by a non-depositional discontinuity (thin blue line) is found in the regressive part.

The studied high-frequency sequences are inferred to be generated by climate-driven changes in sedimentation rates, probably linked to the Milankovitch cyclicity [5,14,47].

6.2. Intra-Sequence Cyclicity

6.2.1. General Characteristics

Internal subdivisions of high-frequency sequences and component systems tracts can be referred to as bedsets, which consist of dm- to m-scale sedimentary units separated by non-depositional or erosional discontinuities, defining individual clinoforms [2,8] (Figure 10). Non-depositional discontinuities are associated with an abrupt upward decrease in thickness and amalgamation of event beds and are related to a decrease in sediment supply and/or energy [2,6]. In contrast, erosional discontinuities record an abrupt upward increase in bed amalgamation and grain size and are inferred to be related to an increase in sediment supply and/or energy [2,6]. Non-depositional and erosional discontinuities resemble flooding surfaces (maximum regressive surfaces, MRSs, or LFSs) and regressive surfaces of marine erosion (RSME), respectively; however, bedset boundaries are more limited laterally and are unrelated to transgressive or regressive shoreline shifts, as they tend to disappear landward in upper shoreface settings (Figure 10) [2,6]. As such, bedsets reflect cycles of internal reorganization of a depositional system, without a change in the systems tract [7].

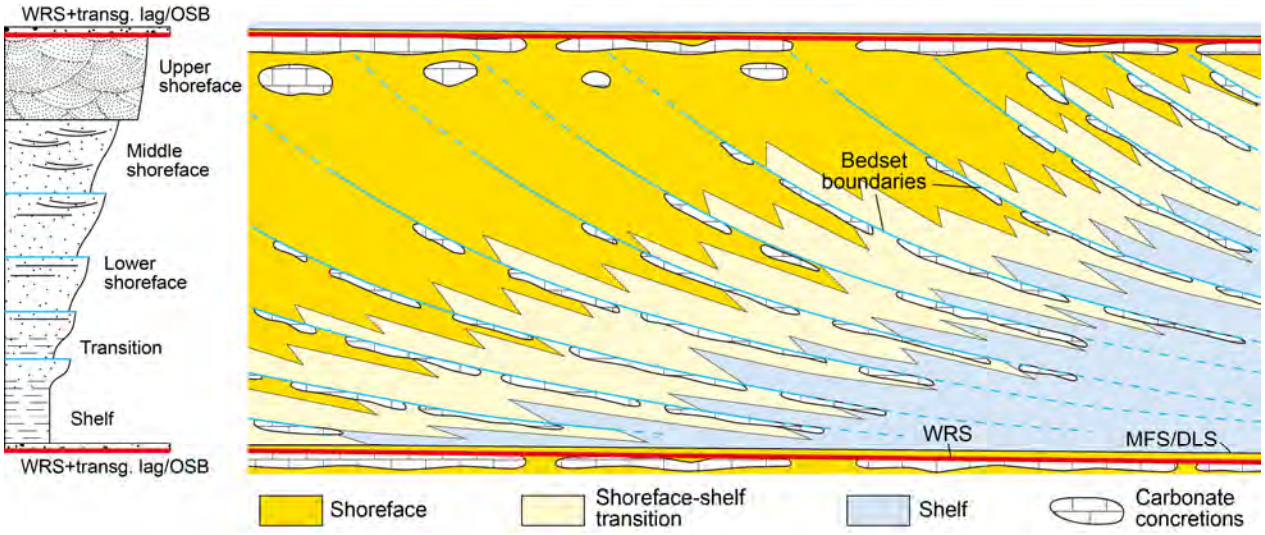

Figure 10. Example of high-frequency sequence dominated by normal regressive deposits (modified from Hampson et al. [76]). Non-depositional discontinuities bounding bedsets, which are highlighted also in the representative section on the left, define clinoforms composing the prograding succession. Bedset boundaries tend to disappear both in proximal and distal directions. Abbreviations: DLS—downlap surface; MFS—maximum flooding surface; OSB—onlap shell bed; WRS—wave-ravinement surface.

In the studied high-frequency sequences, bedsets are locally recognizable; they are ca. 0.5 to 1.8 m thick and can be bounded by non-depositional discontinuities (upper part of the CBS 1 and ZNE 2 sections, Figures 3, 5 and 9) or by erosional discontinuities (lower part of the Strongoli 2 and ZNE 2 sections and Tal section, Figures 4–6, 9 and 11). LFSs may also be considered as non-depositional discontinuities bounding bedsets, although the LFS/DLS pairs, if present, bound CSs and interrupt the bedset stack (Figures 5 and 8B). The WRSs bounding the high-frequency sequences can also act as the base of the first bedset of a sequence, or the top of the last bedset of the underlying sequence (Figures 3–6). Bedsets can be found only occasionally in part of the section (CBS 1 and Strongoli 2 section, Figures 3 and 6) or in the whole section (ZNE 2 and Tal sections, Figures 4, 5, 9 and 11); their lateral continuity along strike ranges from tens to hundreds of meters.

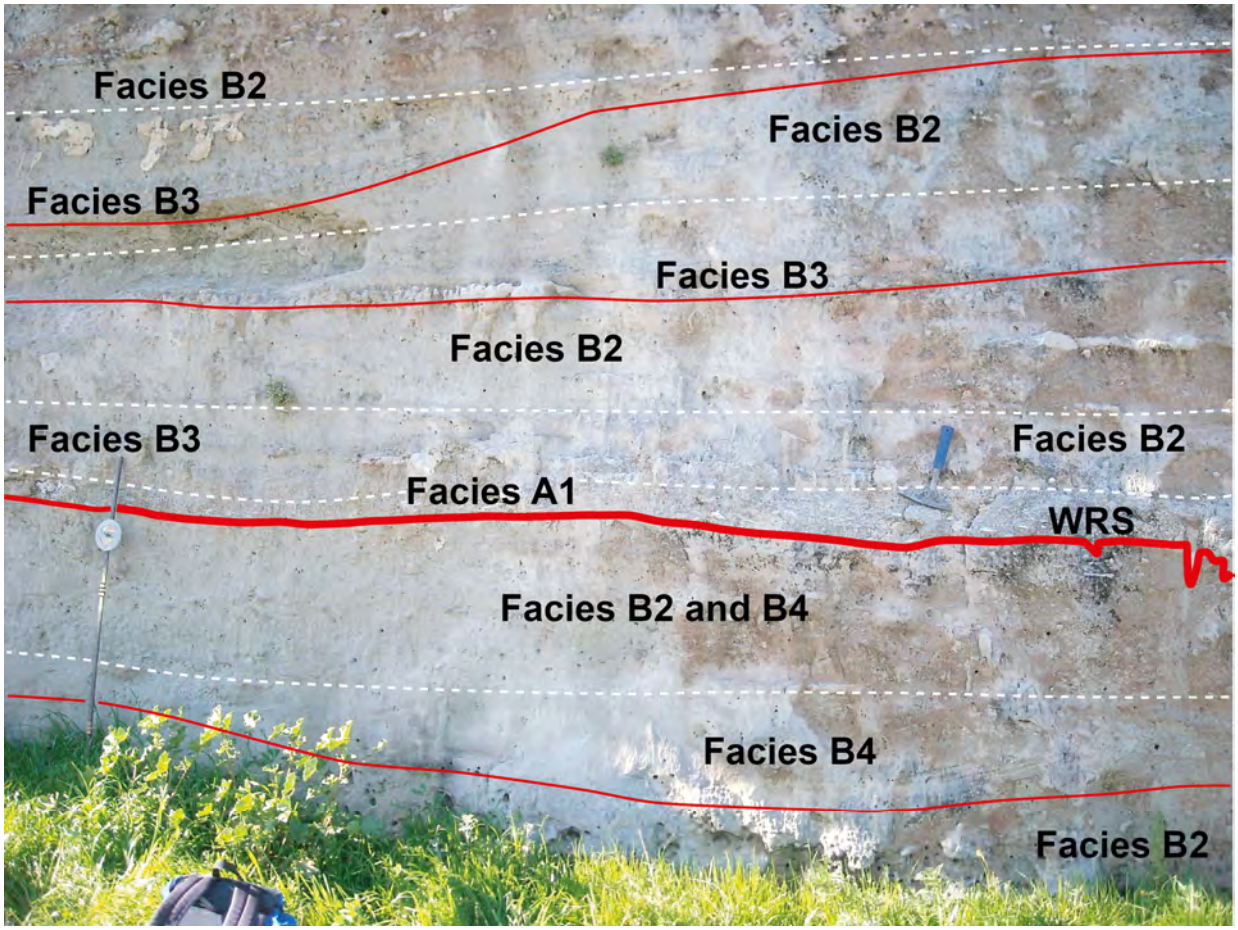

Figure 11. Detail of the TAL section (Figure 4), showing a wave-ravinement surface (WRS) in the middle, separating two high-frequency sequences, and erosional discontinuities (thin red lines) bounding bedsets (see Table 1 for facies code).

Bedsets bounded by non-depositional discontinuities show an upward increase in the degree of amalgamation of storm beds, sparse shells, and grain sizes in the range of Facies B2 to Facies B2/B3 (Figures 3 and 5); in some cases, intense burrowing is found just above the base (Figure 5). Their boundaries are usually placed above storm beds and separate opposite trends of upward increase in storm beds (below) and their sharp decrease across the boundaries (Figures 3, 5 and 9). Bedsets bounded by erosional discontinuities show an upward decrease in the degree of amalgamation of storm beds, or more in general of facies associated with higher energy levels, as documented by a rapid upward shift from Facies B4 or B3 and Facies B2 (Figures 4 and 11), although a persistence of Facies B2 throughout the bedset is also observed (Figures 5 and 9). An upward decrease in grain size and an increase in bioturbation were also observed (Figures 4 and 5). The bedsets boundaries in this case are placed at the base of storm beds or at the basal WRS, and in some cases are marked by the *Glossifungites* Ichnofacies (Figures 4, 5, 9 and 11). Where bedsets are bounded at the base by the WRS, their lower part consists of Facies A1 (Figures 4, 5, 9 and 11).

In general, the studied bedsets meet the sedimentological and stratigraphic criteria highlighted by Zecchin et al. [6] to discriminate sedimentological and stratigraphic cycles, in particular: (1) only minor environmental changes, usually associated with adjacent facies or subfacies changes, are observed across bedset boundaries; (2) water-depth changes usually do not occur across bedset boundaries (with exceptions, see Sections 6.2.2 and 7); (3) bedset boundaries show a more modest physical appearance than the WRSs bounding high-frequency sequences; (4) bedset boundaries have a smaller lateral extent compared

to WRSs; (5) bedset boundaries are not associated with condensed shell beds (except for the first bedset above a WRS or a LFS); (6) in general, bedsets are thinner (dm- to m-scale) than high-frequency sequences (m- to dam-scale); (7) in contrast to sequences, bedsets are not composed of (do not include) clinoforms. As for the micropaleontological and diagenetic criteria reported by Zecchin et al. [6], the former are illustrated and discussed in Sections 6.2.2 and 7, while the latter are exemplified by a modest cementation associated with bedset boundaries, if compared to WRSs and LFSs. Regarding the mineralogical criteria, they were illustrated by Zecchin et al. [5,6], who highlighted that the abundance of heavy minerals in the sediment does not change across bedset boundaries but only across sequence stratigraphic surfaces produced in high-energy conditions. The highest abundance of heavy minerals was invariably found within the OSBs immediately overlying WRSs [5,6].

6.2.2. Relationships with Micropaleontological Parameters

In contrast to high-frequency sequences, in most cases bedsets and their boundaries are not associated with significant changes in the Fr, D/P and P/B parameters that are described in Section 5. In fact, except for the maxima or minima that are recorded close to sequence boundaries and MFSs, the curves of these parameters exhibit minor, erratic variations, which usually seem to be unrelated to bedset boundaries (Figures 3–6).

However, an exception has been observed in the upper part of the ZNE 2 section (Figure 5). Here, the two bedsets composing the HST are separated by a non-depositional discontinuity placed at ca. 4.3 m, above a shell-rich storm bed and below an intensely burrowed interval in Facies B2, marking an abrupt interruption of storm-related event beds (Figure 5). In contrast to what was observed in other situations, in this case a secondary positive peak of both the D/P and P/B parameters is found right at the burrowed interval at ca. 4.7 m, just above the bedset boundary and centered on the Z10 sample (Figure 5). The Fr parameter does not show a significant local variation, but it is still in a relatively thick interval of minimum values that is centered on the MFS of the high-frequency sequence (Figure 5). The significance of these observations is discussed in the next Section.

7. Discussion and Conclusions

Integrated sedimentological and micropaleontological data in selected Zanclean and Gelasian sections of the Crotone Basin have allowed documentation, although discontinuously, of a decimeter-to-meter-scale cyclicity within meter-to-decameter-scale high-frequency sequences inferred to be linked to the Milankovitch cyclicity [14,47] (Figures 3–6).

The lack of correlation between the intra-sequence cycles and the variations in micropaleontological parameters linked to transgressive and regressive trends (i.e., Fr, D/P and P/B; Section 5), in contrast to what is observed for high-frequency sequences [13,14,47,73], strongly suggests that this minor cyclicity is unrelated to shoreline shifts and is probably controlled by local sediment supply and wave-climate changes (e.g., [2,8]). The disconnect from shoreline shifts, in particular, is a key element allowing to classify these minor cycles as bedsets; i.e., sedimentological cycles bounded by either non-depositional or erosional discontinuities, rather than stratigraphic sequences (e.g., [5,7]).

However, the occasional recognition of minor D/P and P/B variations close to bedset boundaries, such as those observed in the upper part of the ZNE 2 section in the Zanclean Belvedere Formation (Figure 5), raises interesting questions. In the ZNE 2 section, both the D/P and P/B parameters show secondary maxima at ca. 4.7 m that follow those associated with maximum flooding and maximum water-depth conditions, respectively, whereas the Fr parameter remains relatively low (Figure 5).

One possibility is that the observed secondary positive peaks, centered on only one sample, are simply erratic variations without any real physical significance. However, the significant value of the D/P parameter at that sample, not much lower than the main peak at ca. 3.2 m, together with the evidence that such a secondary peak falls in an intensely burrowed interval just above the bedset boundary, indicating lower energy levels (Figure 5), would suggest that the secondary peaks of the D/P and P/B parameters are real. In the latter case, since increases in the D/P and P/B parameters indicate transgression and increasing depth, respectively, the non-depositional discontinuity at ca. 4.3 m would be followed by a very minor shoreline transgression, as in the case of an MRS.

Such observations are not really surprising, as the transgressions and regressions that define the high-frequency sequences of the Belvedere Formation are inferred to be controlled by climate-induced changes in sediment supply [14,47], whereas bedsets are in turn likely associated with minor sediment supply changes, much more localized and shorter in duration than sequences, such that associated shoreline shifts are usually not found. It is therefore possible that these minor sediment supply changes may occasionally lead to barely recognizable shoreline shifts that are very modest and more laterally limited than those associated with the sequence that hosts the bedsets.

Another possible explanation relies on the irregularity of the Milankovitch cycles. The trend of the precession, obliquity and eccentricity cycles, in fact, is not sinusoidal and commonly exhibits secondary peaks (e.g., [77,78]). The secondary maxima of the D/P and P/B parameters in the ZNE 2 section (Figure 5), therefore, could record a secondary shoreline transgression and associated MFS within the larger HST regressive phase of the main (higher rank) sequence, and this minor (lower rank) transgression would be still associated with a climatically induced decrease in sediment supply, as for the main TST. Following the stratigraphic sequence concept of Zecchin and Catuneanu [3] and Catuneanu and Zecchin [4], in this hypothesis, the HST of the main sequence found in the ZNE 2 section may consist of two lower rank sequences separated by an MRS, rather than two bedsets. However, in this case only a sub-facies change from storm shell beds to burrowed sandstone is found at ca. 4.3 m (Figure 5), but a transgressive trend is not clearly recognizable on the basis of field data; it is therefore preferred to keep a bedset boundary at 4.3 m, as a working hypothesis, which is more in line with the magnitude and scale of the observed changes. Further work, however, could clarify whether the bedset boundary should be upgraded to the status of a sequence boundary or not.

In contrast to the examples from the CBS 1, Strongoli 2 and TAL sections, where a distinction between bedsets and stratigraphic sequences is clearly recognizable with both sedimentological and micropaleontological criteria (Figures 3, 4 and 6), the evidence found in the ZNE 2 section (Figure 5) is more ambiguous in terms of a clear separation between sedimentologic (bedsets) and stratigraphic cycles. This illustrates that an unequivocal distinction between the two types of cycles may not be possible in all cases, and that a choice one way or the other can be arbitrary in some situations. It is, therefore, suggested that a clear recognition of changes between transgressive and regressive trends by means of field/core observations remains essential in deciding whether meter-scale cycles are lower rank sequences or bedsets. Ambiguity between sedimentological and stratigraphic cycles is implicit in models that consider bedsets as cycles controlled by minor shoreline shifts and deepening/shallowing episodes, which are features that also characterize stratigraphic sequences, and/or illustrate a hierarchy of bedsets and sets of bedsets that blur the distinction between sedimentological and stratigraphic cycles [9,10]. Both shoreline reorganizations and minor relative sea-level changes as possible controlling mechanisms on bedset boundaries are also advocated by Sømme et al. [8].

In any case, irrespective of the preferred terminology, cycles with intermediate features between high-frequency sequences (*sensu* Zecchin and Catuneanu [3] and Catuneanu and Zecchin [4]) and sedimentological cycles exist and share characteristics of both, testifying to the passage between sedimentology and stratigraphy.

Supplementary Materials: The following supporting information can be downloaded at: https://www.mdpi.com/article/10.3390/geosciences16020089/s1, Table S1: Number of benthic microforaminifera specimens found in the samples collected along the measured sections.

Author Contributions: Conceptualization, M.Z. and O.C.; Methodology, M.Z. and M.C.; Software, M.Z.; Validation, M.Z. and M.C.; Formal analysis, M.Z. and M.C.; Investigation, M.Z., M.C. and O.C.; Resources, M.C.; Data curation, M.C.; Writing—original draft, M.Z.; Writing—review and editing, M.Z., M.C. and O.C.; Visualization, M.Z.; Supervision, M.Z. and O.C.; Project administration, M.Z. All authors have read and agreed to the published version of the manuscript.

Funding: This research received no funding.

Data Availability Statement: The original contributions presented in this study are included in the article/Supplementary Materials. Further inquiries can be directed to the corresponding author(s).

Conflicts of Interest: The authors declare no conflicts of interest.

References

1. Van Wagoner, J.C.; Mitchum, R.M.; Campion, K.M.; Rahmanian, V.D. *Siliciclastic Sequence Stratigraphy in Well Logs, Cores, and Outcrops*; AAPG Methods in Exploration; American Association of Petroleum Geologists: Tulsa, OK, USA, 1990; Volume 7, p. 55.
2. Hampson, G.J. Discontinuity surfaces, clinoforms, and facies architecture in a wave-dominated, shoreface-shelf parasequence. *J. Sediment. Res.* **2000**, *70*, 325–340. [CrossRef]
3. Zecchin, M.; Catuneanu, O. High-resolution sequence stratigraphy of clastic shelves I: Units and bounding surfaces. *Mar. Pet. Geol.* **2013**, *39*, 1–25. [CrossRef]
4. Catuneanu, O.; Zecchin, M. High-resolution sequence stratigraphy of clastic shelves II: Controls on sequence development. *Mar. Pet. Geol.* **2013**, *39*, 26–38. [CrossRef]
5. Zecchin, M.; Caffau, M.; Catuneanu, O.; Lenaz, D. Discrimination between wave-ravinement surfaces and bedset boundaries in Pliocene shallow-marine deposits, Crotone Basin, southern Italy: An integrated sedimentological, micropaleontological and mineralogical approach. *Sedimentology* **2017**, *64*, 1755–1791. [CrossRef]
6. Zecchin, M.; Catuneanu, O.; Caffau, M. High-resolution sequence stratigraphy of clastic shelves V: Criteria to discriminate between stratigraphic sequences and sedimentological cycles. *Mar. Pet. Geol.* **2017**, *85*, 259–271. [CrossRef]
7. Catuneanu, O. *Principles of Sequence Stratigraphy*, 2nd ed.; Elsevier: Amsterdam, The Netherlands, 2022; p. 494.
8. Sømme, T.O.; Howell, J.A.; Hampson, G.J.; Storms, J.E.A. Genesis, architecture, and numerical modeling of intra-parasequence discontinuity surfaces in wave-dominated deltaic deposits: Upper Cretaceous Sunnyside Member, Blackhawk Formation, Book Cliffs, Utah, U.S.A. In *Recent Advances in Models of Siliciclastic Shallow-Marine Stratigraphy*; Hampson, G.J., Steel, R.J., Burgess, P.M., Dalrymple, R.W., Eds.; SEPM Special Publication: Claremore, OK, USA, 2008; Volume 90, pp. 421–441.
9. Ainsworth, R.B.; Vakarelov, B.K.; MacEachern, J.A.; Rarity, F.; Lane, T.I.; Nanson, R.A. Anatomy of a shoreline regression: Implications for the high-resolution stratigraphic architecture of deltas. *J. Sediment. Res.* **2017**, *87*, 425–459. [CrossRef]
10. Isla, M.F.; Coronel, M.D.; Schwarz, E.; Veiga, G.D. Depositional architecture of a wave-dominated clastic shoreline (Pilmatué Member, Argentina): Linking dynamics and stratigraphic record of bar-trough systems. *Mar. Pet. Geol.* **2020**, *118*, 104417. [CrossRef]
11. Van Dijk, J.P.; Okkes, F.W.M. Neogene tectonostratigraphy and kinematics of Calabrian basins; implications for the geodynamics of the Central Mediterranean. *Tectonophysics* **1991**, *196*, 23–60. [CrossRef]
12. Zecchin, M.; Massari, F.; Mellere, D.; Prosser, G. Anatomy and evolution of a Mediterranean-type fault bounded basin: The Lower Pliocene of the northern Crotone Basin (Southern Italy). *Basin Res.* **2004**, *16*, 117–143. [CrossRef]
13. Zecchin, M.; Caffau, M.; Catuneanu, O. Identification of maximum flooding surfaces at different scales: The case of the Piacenzian to Gelasian Cutro Clay and Strongoli Sandstone (Crotone Basin, southern Italy). *Mar. Pet. Geol.* **2022**, *146*, 105971. [CrossRef]
14. Zecchin, M.; Caffau, M.; Catuneanu, O. Recognizing maximum flooding surfaces in shallow-water deposits: An integrated sedimentological and micropaleontological approach (Crotone Basin, southern Italy). *Mar. Pet. Geol.* **2021**, *133*, 105225. [CrossRef]

15. Zecchin, M.; Civile, D.; Caffau, M.; Critelli, S.; Muto, F.; Mangano, G.; Ceramicola, S. Sedimentary evolution of the Neogene-Quaternary Crotone Basin (southern Italy) and relationships with large-scale tectonics: A sequence stratigraphic approach. *Mar. Pet. Geol.* **2020**, *117*, 104381. [CrossRef]
16. Cita, M.B. Studi sul Pliocene e sugli strati di passaggio dal Miocene al Pliocene. VIII. Planktonic foraminiferal biozonation of the Mediterranean Pliocene deep-sea record. A revision. *Riv. Ital. Di Paleontol. E Stratigr.* **1975**, *81*, 527–544.
17. Rio, D.; Raffi, I.; Villa, G. Pliocene-Pleistocene calcareous nannofossil distribution patterns in the Western Mediterranean. *Proc. Ocean Drill. Program Sci. Results* **1990**, *107*, 513–533.
18. Lourens, L.J.; Antonarakou, A.; Hilgen, F.J.; Van Hoof, A.A.M.; Vergnaud-Grazzini, C.; Zachariasse, W.J. Evaluation of the Plio-Pleistocene astronomical timescale. *Paleoceanography* **1996**, *11*, 391–413. [CrossRef]
19. Raffi, I.; Backman, J.; Fornaciari, E.; Pälike, H.; Rio, D.; Lourens, L.; Hilgen, F. A review of calcareous nannofossil astrobiochronology encompassing the past 25 million years. *Quat. Sci. Rev.* **2006**, *25*, 3113–3137. [CrossRef]
20. Amodio Morelli, L.; Bonardi, G.; Colonna, V.; Dietrich, D.; Giunta, G.; Ippolito, F.; Liguori, V.; Lorenzoni, S.; Paglionico, A.; Perrone, V.; et al. L'Arco Calabro-Peloritano nell'orogene Appenninico-Maghrebide. *Mem. Della Soc. Geol. Ital.* **1976**, *17*, 1–60.
21. Van Dijk, J.P.; Bello, M.; Brancaleoni, G.P.; Cantarella, G.; Costa, V.; Frixa, A.; Golfetto, F.; Merlini, S.; Riva, M.; Torricelli, S.; et al. A regional structural model for the northern sector of the Calabrian Arc (southern Italy). *Tectonophysics* **2000**, *324*, 267–320. [CrossRef]
22. Bonardi, G.; Cavazza, W.; Perrone, V.; Rossi, S. Calabria–Peloritani terrane and northern Ionian Sea. In *Anatomy of an Orogen: The Apennines and Adjacent Mediterranean Basins*; Vai, G.B., Martini, I.P., Eds.; Kluwer Academic Publishers: Bodmin, UK, 2001; pp. 287–306.
23. Malinverno, A.; Ryan, W.B.F. Extension in the Tyrrhenian Sea and shortening in the Apennines as a result of arc migration driven by sinking of the lithosphere. *Tectonics* **1986**, *5*, 227–245. [CrossRef]
24. Faccenna, C.; Becker, T.W.; Lucente, F.P.; Jolivet, L.; Rossetti, F. History of subduction and back-arc extension in the Central Mediterranean. *Geophys. J. Int.* **2001**, *145*, 809–820. [CrossRef]
25. Faccenna, C.; Civetta, L.; D'Antonio, M.; Funiciello, F.; Margheriti, L.; Piromallo, C. Constraints on mantle circulation around the deforming Calabrian slab. *Geophys. Res. Lett.* **2005**, *32*, L06311. [CrossRef]
26. Sartori, R. The Tyrrhenian back-arc basin and subduction of the Ionian lithosphere. *Episodes* **2003**, *26*, 217–221. [CrossRef] [PubMed]
27. Guillaume, B.; Funiciello, F.; Faccenna, C.; Martinod, J.; Olivetti, V. Spreading pulses of the Tyrrhenian Sea during the narrowing of the Calabrian slab. *Geology* **2010**, *38*, 819–822. [CrossRef]
28. Critelli, S. Provenance of Mesozoic to Cenozoic Circum-Mediterranean sandstones in relation to tectonic setting. *Earth-Sci. Rev.* **2018**, *185*, 624–648. [CrossRef]
29. Tripodi, V.; Muto, F.; Brutto, F.; Perri, F.; Critelli, S. Neogene-quaternary evolution of the forearc and backarc regions between the Serre and Aspromonte Massifs, Calabria (southern Italy). *Mar. Pet. Geol.* **2018**, *95*, 328–343. [CrossRef]
30. Critelli, S.; Martín-Martín, M. Provenance, Paleogeographic and paleotectonic interpretations of Oligocene-Lower Miocene sandstones of the western-central Mediterranean region: A review. *J. Asian Earth Sci. X* **2022**, *8*, 100124. [CrossRef]
31. Critelli, S.; Martín-Martín, M. History of western Tethys Ocean and the birth of the circum-Mediterranean orogeny as reflected by source-to-sink relations. *Int. Geol. Rev.* **2024**, *66*, 505–515. [CrossRef]
32. Roda, C. Distribuzione e facies dei sedimenti Neogenici nel Bacino Crotonese. *Geol. Romana* **1964**, *3*, 319–366.
33. Van Dijk, J.P. Sequence stratigraphy, kinematics and dynamic geohistory of the Crotone Basin (Calabria arc, central mediterranean): An integrated approach. *Mem. Della Soc. Geol. Ital.* **1990**, *44*, 259–285.
34. Zecchin, M.; Mellere, D.; Roda, C. Sequence stratigraphy and architectural variability in growth fault-bounded basin fills: A review of Plio-Pleistocene stratal units of the Crotone Basin, southern Italy. *J. Geol. Soc.* **2006**, *163*, 471–486. [CrossRef]
35. Zecchin, M.; Caffau, M.; Civile, D.; Critelli, S.; Di Stefano, A.; Maniscalco, R.; Muto, F.; Sturiale, G.; Roda, C. The Plio-Pleistocene evolution of the Crotone Basin (southern Italy): Interplay between sedimentation, tectonics and eustasy in the frame of Calabrian Arc migration. *Earth Sci. Rev.* **2012**, *115*, 273–303. [CrossRef]
36. Massari, F.; Prosser, G. Late Cenozoic tectono-stratigraphic sequences of the Crotone Basin: Insights on the geodynamic history of the Calabrian arc and Tyrrhenian Sea. *Basin Res.* **2013**, *25*, 26–51. [CrossRef]
37. Criniti, S.; Borrelli, M.; Falsetta, E.; Civitelli, M.; Pugliese, E.; Arcuri, N. Sandstone petrology of the Crotone basin, Calabria (Italy) from well cores. *Rend. Online Della Soc. Geol. Ital.* **2023**, *59*, 64–70. [CrossRef]
38. Mangano, G.; Zecchin, M.; Civile, D.; Critelli, S. Tectonic evolution of the Crotone Basin (central Mediterranean): The important role of two strike-slip fault zones. *Mar. Pet. Geol.* **2024**, *163*, 106769. [CrossRef]
39. Zecchin, M.; Caffau, M.; Di Stefano, A.; Maniscalco, R.; Lenaz, D.; Civile, D.; Muto, F.; Critelli, S. The Messinian succession of the Crotone Basin (southern Italy) II: Facies architecture and stratal surfaces across the Miocene-Pliocene boundary. *Mar. Pet. Geol.* **2013**, *48*, 474–492. [CrossRef]

40. Zecchin, M.; Civile, D.; Caffau, M.; Muto, F.; Di Stefano, A.; Maniscalco, R.; Critelli, S. The Messinian succession of the Crotone Basin (southern Italy) I: Stratigraphic architecture reconstructed by seismic and well data. *Mar. Pet. Geol.* **2013**, *48*, 455–473. [CrossRef]
41. Zecchin, M.; Praeg, D.; Ceramicola, S.; Muto, F. Onshore to offshore correlation of regional unconformities in the Plio-Pleistocene sedimentary successions of the Calabrian Arc (central Mediterranean). *Earth-Sci. Rev.* **2015**, *142*, 60–78. [CrossRef]
42. Gliozzi, E. I terrazzi del Pleistocene superiore della Penisola di Crotone (Calabria). *Geol. Romana* **1987**, *26*, 17–79.
43. Cosentino, D.; Gliozzi, E.; Salvini, F. Brittle deformations in the Upper Pleistocene deposits of the Crotone Peninsula, Calabria, southern Italy. *Tectonophysics* **1989**, *163*, 205–217. [CrossRef]
44. Zecchin, M.; Nalin, R.; Roda, C. Raised Pleistocene marine terraces of the Crotone peninsula (Calabria, southern Italy): Facies analysis and organization of their deposits. *Sediment. Geol.* **2004**, *172*, 165–185. [CrossRef]
45. Zecchin, M.; Caffau, M.; Ceramicola, S. Interplay between regional uplift and glacio-eustasy in the Crotone Basin (Calabria, southern Italy) since 0.45 Ma: A review. *Glob. Planet. Change* **2016**, *143*, 196–213. [CrossRef]
46. Loeblich, A.R.; Tappan, H. *Foraminiferal Genera and Their Classification*; Van Nostrand Reinhold Company: New York, NY, USA, 1987; p. 970.
47. Zecchin, M.; Caffau, M.; Catuneanu, O. Zanclean to Gelasian high-frequency sequences of the Crotone Basin (southern Italy): Architectural variability and forcing mechanisms. *Mar. Pet. Geol.* **2024**, *162*, 106753. [CrossRef]
48. Kidwell, S.M. Condensed deposits in siliciclastic sequences: Expected and observed features. In *Cycles and Events in Stratigraphy*; Einsele, G., Ricken, W., Seilacher, A., Eds.; Springer: Berlin/Heidelberg, Germany, 1991; pp. 682–695.
49. Norris, R.D. Taphonomic gradients in shelf fossil assemblages: Pliocene Purisima Formation, California. *Palaios* **1986**, *1*, 256–270. [CrossRef]
50. Zecchin, M.; Catuneanu, O.; Caffau, M. Wave-ravinement surfaces: Classification and key characteristics. *Earth Sci. Rev.* **2019**, *188*, 210–239. [CrossRef]
51. Kidwell, S.M.; Fürsich, F.T.; Aigner, T. Conceptual framework for the analysis and classification of fossil concentrations. *Palaios* **1986**, *1*, 228–238. [CrossRef]
52. Cantalamessa, G.; Di Celma, C.; Ragaini, L. Sequence stratigraphy of the Punta Ballena Member of the Jama Formation (Early Pleistocene, Ecuador): Insights from integrated sedimentologic, taphonomic and paleoecologic analysis of molluscan shell concentrations. *Palaeogeogr. Palaeoclimatol. Palaeoecol.* **2005**, *216*, 1–25. [CrossRef]
53. Clifton, H.E. A reexamination of facies models for clastic shorelines. In *Facies Models Revisited*; Posamentier, H.W., Walker, R.G., Eds.; SEPM Society for Sedimentary Geology: Claremore, OK, USA, 2006; Volume 84, pp. 293–337.
54. Galloway, W.E.; Hobday, D.K. *Terrigenous Clastic Depositional Systems—Applications to Fossil Fuel and Groundwater Resources*, 2nd ed.; Springer: New York, NY, USA, 1996; p. 489.
55. Reading, H.G.; Collinson, J.D. Clastic Coasts. In *Sedimentary Environments; Processes, Facies and Stratigraphy*; Reading, H.G., Ed.; Blackwell Science: Oxford, UK, 1996; pp. 154–231.
56. Dott, R.H.; Bourgeois, J. Hummocky stratification: Significance of its variable bedding sequences. *Geol. Soc. Am. Bull.* **1982**, *93*, 663–680. [CrossRef]
57. Dumas, S.; Arnott, R.W.C.; Southard, J.B. Experiments on oscillatory-flow and combined-flow bed forms: Implications for interpreting parts of the shallow-marine sedimentary record. *J. Sediment. Res.* **2005**, *75*, 501–513. [CrossRef]
58. Leckie, D.A.; Walker, R.G. Storm- and tide-dominated shorelines in Cretaceous Moosebar-Lower Gates interval-outcrop equivalents of deep basin gas trap in Western Canada. *AAPG Bull.* **1982**, *66*, 138–157.
59. Massari, F.; Parea, G.C. Progradational gravel beach sequences in a moderate- to high-energy, microtidal marine environment. *Sedimentology* **1988**, *35*, 881–913. [CrossRef]
60. Hart, B.S.; Plint, A.G. Gravelly shoreface and beachface deposits. In *Sedimentary Facies Analysis; International Association of Sedimentologists Special Publication*; Plint, A.G., Ed.; John Wiley & Sons, Inc.: Hoboken, NJ, USA, 1995; Volume 22, pp. 75–99.
61. Zecchin, M. Relationships between fault-controlled subsidence and preservation of shallow-marine small-scale cycles: Example from the lower Pliocene of the Crotone Basin (southern Italy). *J. Sediment. Res.* **2005**, *75*, 300–312. [CrossRef]
62. Capraro, L.; Consolaro, C.; Fornaciari, E.; Massari, F.; Rio, D. Chronology of the middle-upper Pliocene succession in the Strongoli area: Constraints on the geological evolution of the Crotone Basin (southern Italy). In *Tectonics of the Western Mediterranean and North Africa; Geological Society Special Publication 2006*; Moratti, G., Chalouan, A., Eds.; Geological Society of London: London, UK, 2006; Volume 262, pp. 323–336.
63. Abbott, S.T. Foraminiferal paleobathymetry and mid-cycle architecture of mid-Pleistocene depositional sequences, Wanganui Basin, New Zealand. *Palaios* **1997**, *12*, 267–281. [CrossRef]
64. Naish, T.R.; Kamp, P.J.J. Foraminiferal depth palaeoecology of Late Pliocene shelf sequences and system tracts, Wanganui Basin, New Zealand. *Sediment. Geol.* **1997**, *110*, 237–255. [CrossRef]
65. Donnici, S.; Serandrei-Barbero, R. The benthic foraminiferal communities of the North Adriatic continental shelf. *Mar. Micropaleontol.* **2002**, *44*, 93–123. [CrossRef]

66. Mendes, I.; Gonzalez, R.; Dias, J.M.A.; Lobo, F.; Martins, V. Factors influencing recent benthic foraminifera distribution on the Guadiana shelf (Southwestern Iberia). *Mar. Micropaleontol.* **2004**, *51*, 171–192. [CrossRef]
67. Stefanelli, S. Benthic foraminiferal assemblages as tools for paleoenvironmental reconstruction of the early-middle Pleistocene Motalbano Jonico composite section. *Boll. Della Soc. Paleontol. Ital.* **2003**, *42*, 281–299.
68. Morigi, C.; Jorissen, F.J.; Fraticelli, S.; Horton, B.P.; Principi, M.; Sabbatini, A.; Capotondi, L.; Curzi, P.V.; Negri, A. Benthic foraminiferal evidence for the formation of the Holocene mud-belt and bathymetrical evolution in the central Adriatic Sea. *Mar. Micropaleontol.* **2005**, *57*, 25–49. [CrossRef]
69. Phipps, M.D.; Kaminiski, M.A.; Aksu, A.E. Calcareous benthic foraminiferal biofacies along a depth transect on the southwestern marmara shelf (Turkey). *Micropaleontology* **2010**, *56*, 377–392. [CrossRef]
70. Frezza, V.; Carboni, M.G. Distribution of recent foraminiferal assemblages near the Ombrone River mouth (Northern Tyrrhenian Sea, Italy). *Rev. Micropaléontologie* **2009**, *52*, 43–66. [CrossRef]
71. Rossi, V.; Barbieri, G.; Vaiani, S.C.; Amorosi, A. Benthic foraminifers from Holocene subaqueous deltas of the Western Mediterranean: Stratigraphic implications and palaeoenvironmental significance of the biofacies. *Mar. Geol.* **2021**, *442*, 106632. [CrossRef]
72. Jamrich, M.; Rybár, S.; Ruman, A.; Kováčová, M.; Hudáčková, N. Biostratigraphy and paleoecology of the upper Badenian carbonate and siliciclastic nearshore facies in the Vienna Basin (Slovakia). *Facies* **2024**, *70*, 5. [CrossRef]
73. Zecchin, M.; Catuneanu, O.; Caffau, M. High-resolution sequence stratigraphy of clastic shelves IX: Methods for recognizing maximum flooding conditions in shallow-marine settings. *Mar. Pet. Geol.* **2023**, *156*, 106468. [CrossRef]
74. Naish, T.R.; Kamp, P.J.J. Sequence stratigraphy of sixth-order (41 k.y.) Pliocene-Pleistocene cyclothems, Wanganui basin, New Zealand: A case for the regressive systems tract. *Geol. Soc. Am. Bull.* **1997**, *109*, 978–999. [CrossRef]
75. Kondo, Y.; Abbott, S.T.; Kitamura, A.; Kamp, P.J.J.; Naish, T.R.; Kamataki, T.; Saul, G.S. The relationship between shell bed type and sequence architecture: Examples from Japan and New Zealand. *Sediment. Geol.* **1998**, *122*, 109–127. [CrossRef]
76. Hampson, G.J.; Rodriguez, A.B.; Storms, J.E.A.; Johnson, H.D.; Meyer, C.T. Geomorphology and high-resolution stratigraphy of progradational wave-dominated shoreline deposits: Impact on reservoir-scale facies architecture. In *Recent Advances in Models of Siliciclastic Shallow-Marine Stratigraphy; SEPM Special Publication 2008*; Hampson, G.J., Steel, R.J., Burgess, P.M., Dalrymple, R.W., Eds.; SEPM Society for Sedimentary Geology: Claremore, OK, USA, 2008; Volume 90, pp. 117–142.
77. Shackleton, N.J.; Hall, M.A.; Pate, D. Pliocene stable isotope stratigraphy of ODP Site 846. *Proc. Ocean. Drill. Program Sci. Results* **1995**, *138*, 337–356.
78. Lisiecki, L.E.; Raymo, M.E. A Pliocene-Pleistocene stack of 57 globally distributed benthic δ18O records. *Paleoceanography* **2005**, *20*, PA1003. [CrossRef]